Multimodal AGuIX® Nanoparticles: Size Characterization by HF5 and Optimization of the Radiolabeling with Various SPECT/PET/Theranostic Tracers

S. Huclier-Markai, E. Ntsiba, Eloise Thomas, C. Alliot, Cs Cutler, F. Lux, O. Tillement

ISSN: 2378-3664

Huclier-Markai et al. Int J Med Nano Res 2019, 6:027
DOI: 10.23937/2378-3664.1410027
Volume 6 | Issue 1
Open Access

International Journal of
Medical Nano Research

RESEARCH ARTICLE

Multimodal AGuIX® Nanoparticles: Size Characterization by HF5 and Optimization of the Radiolabeling with Various SPECT/PET/Theranostic Tracers

S Huclier-Markai[1,2], E Ntsiba[1], E Thomas[3], C Alliot[2,4], CS Cutler[5], F Lux and O Tillement[3*]*

[1]SUBATECH, UMR 6457, IMT Atlantique/CNRS-IN2P3/Université de Nantes, 4 Rue Alfred Kastler La Chantrerie, BP 20722, 44307 Nantes Cedex 3, France

[2]ARRONAX, 1 Rue Aronnax-CS 10112-44817 Saint-Herblain Cedex, France

[3]Université Claude Bernard Lyon 1, CNRS, Institut Lumière Matière, F-69622, LYON, France

[4]CRCNA -INSERM U892, 9 Quai Moncousu, 44035 Nantes Cedex 01, France

[5]Brookhaven National Laboratory, 801 Rutherford Drive, Upton, NY 11973, USA

***Corresponding author:** S Huclier-Markai, SUBATECH, UMR 6457, IMT Atlantique/CNRS-IN2P3/Université de Nantes, 4 rue Alfred Kastler La Chantrerie, BP 20722, 44307 Nantes Cedex 3, France

Abstract

Diagnostics that combine imaging techniques such as PET and MRI could enhance disease detection and location if effective multimodal contrast agents can be developed. A nanoparticle called AGuIX has been developed that is comprised of gadolinium-bound by chelates and additional free chelates that can be further labelled with radioactive isotopes enabling both PET and MRI imaging.

Herein, we describe the size characterization of these nanoparticles together with their size distribution, which is an important parameter for pharmacokinetics, by a hyphenated method that is hollow fiber flow field flow fractionation (HF5). Once radiolabeled, the size was determined to confirm their integrity. The average radius of these nanoparticles was about 3.5 nm and was not significantly affected by radiolabeling.

The labeling of these nanoparticles with radionuclides for SPECT/PET was also evaluated (namely ^{64}Cu, ^{44}Sc and ^{67}Ga). Parameters such as the molar ratio, pH and temperature were optimized. For the three radionuclides considered, 60% to 100% radiolabeling yields were reached, with no further purification at this stage. High specific activities could be attainable for all percentages of free DOTA grafted at the surface of the AGuIX nanoparticles considered in this work.

Keywords

Nanoparticles, Multimodality, Radiolabeling, AguiX, Scandium-44, Copper-64, Gallium-67

Introduction

Drug delivery systems comprised of nanoparticles are already being used in the clinic as carriers for sensitive chemotherapeutics or highly toxic substances, are an emerging field for imaging and therapy of tumors able to carry and deliver radionuclides for therapeutic or imaging purposes [1]. Gadolinium-based nanoparticles (GBN) have been developed and can be detected by MRI and PET imaging modalities used in routine clinical practice. Additionally, they can be used as radio sensitizing agents in cancer therapy [2]. These GBN, called AGuIX, are composed of a polysiloxane backbone conjugated to DOTA (1,4,7,10-tetraazacyclododecane-1,4,7,10-tetraacetic acid) derivatives. These DOTA complexes are covalently bound at the surface of the particle via an amide bond [2]. After 2 days of maturation in water (final step of purification process), the Gd_2O_3 core is totally dissolved by a top-down process described in detail by Le Duc, et al. [3], where the presence of the chelate is crucial to reduce the nanoparticles hydrodynamic diameter from 10 nm to approximately 3-5 nm nanoparticles and promote the dissolution of Gd_2O_3.

One of the limitations for the translation of nanoparticles to the clinic is toxicity. The advantage of

Citation: Huclier-Markai S, Ntsiba E, Thomas E, Alliot C, Cutler CS, et al. (2019) Multimodal AGuIX® Nanoparticles: Size Characterization by HF5 and Optimization of the Radiolabeling with Various SPECT/PET/Theranostic Tracers. Int J Med Nano Res 6:027. doi.org/10.23937/2378-3664/1410027

Accepted: February 23, 2019: **Published:** February 25, 2019

ultra-small GBN nanoparticles is their biodegradability and renal elimina-tion that limits the risk of toxicity [4]. Furthermore, the 3-5 nm size of these nanoparticles enables clearance via the kidneys [4-6]. These NPs exhibit two-fold higher plasmatic res-idence time than DOTAREM® in rodents (commercial MRI contrast agent) and display significant accumulation in tumor tissues thus suggesting Enhanced Permeability and Retention (EPR) effect [7].

In addition, to target a tumor, these nanoparticles can be functionalized with different binding moieties such as amine, thiol, carboxylic or methacrylate and a targeting molecule can be conjugated through the selected linker [8,9]. For instance, targeting molecules such as cRGD, ATWLPPR have been proposed to target malignant cells or neovesssels [10,11]. Peptides highly specific for Aβ amyloid fibrils in the case of Alzheimer disease have also been proposed [12]. The carboxylic acid groups of DOTA on GBN surface can also bind aromatic quaternary ammonium (QA) functions and increase the accumulation in the tumor site in the case of chondrosarcoma. These QA have equally affinity for sulfate and carboxylate groups in the glycosamynoglycan moieties on proteoglycans overexpressed in malignant cells [13].

Moreover, DOTA is a universal chelator for radiometals that has been shown to be a good chelate for binding M^{3+} and M^{2+} radiometals with high kinetic and thermodynamic stability for avoiding *in-vivo* transmetallation and subsequent damage to normal tissue [14,15]. These GBN exhibit sensitizing properties, which render them hopeful therapeutic agents for radiotherapy [16,17] and have recently been demonstrated to be an efficient theranostic tool for image-guided radiation therapy of brain tumors [14].

The continuous quest to improve diagnostic performance and optimize treatment strategies has led to the development of combined imaging modalities: the high spatial and contrast resolution of MRI with the high sensitivity and molecular functional information from PET imaging. The use of positron emission tomography (PET)/magnetic resonance imaging (MRI) is mainly because of its ability to provide complementary functional, morphological, molecular, and (patho-) physiological information related to the pathology. This will ultimately lead to a better stratification of patients before therapies, selection of patient candidates, thus, avoiding both toxicity issues and cost of an ineffective therapy. GBN are good candidate as regard of gadolinium core allowing MRI and DOTA chelate allowing chelation of radiometals used for PET.

DOTAs grafted at the surface are used to bind essentially Gd^{3+} for MRI imaging. The quantity of free DOTAs, expressed in percentages by reference to the number of DOTA complexed with Gd^{3+} ions, are available to complex a metallic radioisotope (e.g. ^{67}Ga,^{64}Cu,^{44}Sc) for SPECT/CT or PET/CT imaging [18]. The final quantity of free DOTA is expressed in percentages by reference to the number of DOTA complexed with Gd^{3+} ions. Even if the quantity of free DOTA is low, it is sufficient for radio imaging that is very sensitive. The number of free ligands can be increased by post-functionalization or slight modification in the synthetic process.

^{99m}Tc is the most employed metallic radionuclide (RN) in SPECT imaging whereas the gold standard for PET is ^{18}F. Another recently established radioisotope for PET is 68Ga ($T_{1/2}$ = 68 min) with a half-life comparable to ^{18}F, it has a metallic character which facilitates radiolabeling and can be acquired from an in-house generator that can be eluted every 4 hours, thus eliminating the need for an on-site cyclotron. Even though numerous radiopharmaceuticals are available for imaging, certain medicinal applications require RN with a longer half-life. Longer RN half-lives ($T_{½}$) is translated to a longer time for *in-vivo* target accumulation and, leads to enhanced inter-tissue resolution and image quality. It is especially the case for radiopharmaceuticals with slow pharmacokinetics. Emerging PET RN with longer half-lives are notably ^{44}Sc ($T_{1/2}$ = 3.97 h), ^{64}Cu ($T_{1/2}$ = 12.7 h) and ^{89}Zr ($T_{1/2}$ = 78.41 hrs). In addition, these radionuclides serve as matched imaging iso-topes for tailored therapeutic agents and are named theranostic agents [19]. A theranostic agent in nuclear medicine is one that binds an isotope for both imaging and therapeutic purposes like ^{44}Sc/^{47}Sc or ^{43}Sc/^{47}Sc [19]. The theranostic approach, which is achieved by switching the diagnostic radionuclide with the therapeutic one on the same chelating system [20,21] could also be performed on nanodimensional structures such as GBN. ^{64}Cu (β^+ 17.6%, β^- 38.5%, and EC 43.9%) is an attractive radionuclide in nuclear medicine for both PET but still with some disadvantages (only 17.6% branching ratio of β^+) [22] and radiotherapy. The lower β energy for ^{64}Cu is convenient for small tumors but the issue with *in-vivo* reduction to Cu(I) has been addressed through the development of more stable chelators [11,23].

^{44}Sc is another attractive PET RN, with a half-life compatible to the pharmacokinetics of a wide range of targeting vectors (such as peptides, antibody fragments and oligonucleotides). The validity, usefulness and advantages of ^{44}Sc have been demonstrated by examples featuring ^{44}Sc-radiolabeled targeting vectors, including ^{44}Sc-radiopharmaceuticals evaluated nowadays in patients. Its low-energy positron emission like F-18 ensures a high image resolution. One should bear in mind that the ^{44m}Sc isomer could be of interest, as its longer half-life ($T_{½}$ = 58.6 h) permits imaging at later times for more accurate assessment of distribution and absorbed doses with high molecular weight targeting vectors, such as antibodies or F(ab')2 antibody fragments, whose biological half-lives are in the order of a few days. As the ^{44m}Sc decay is of very low energy, it can be used as an *in-vivo* $^{44m/44}Sc$ generator [24] and the *in-vivo* ^{44}Sc utiliza-

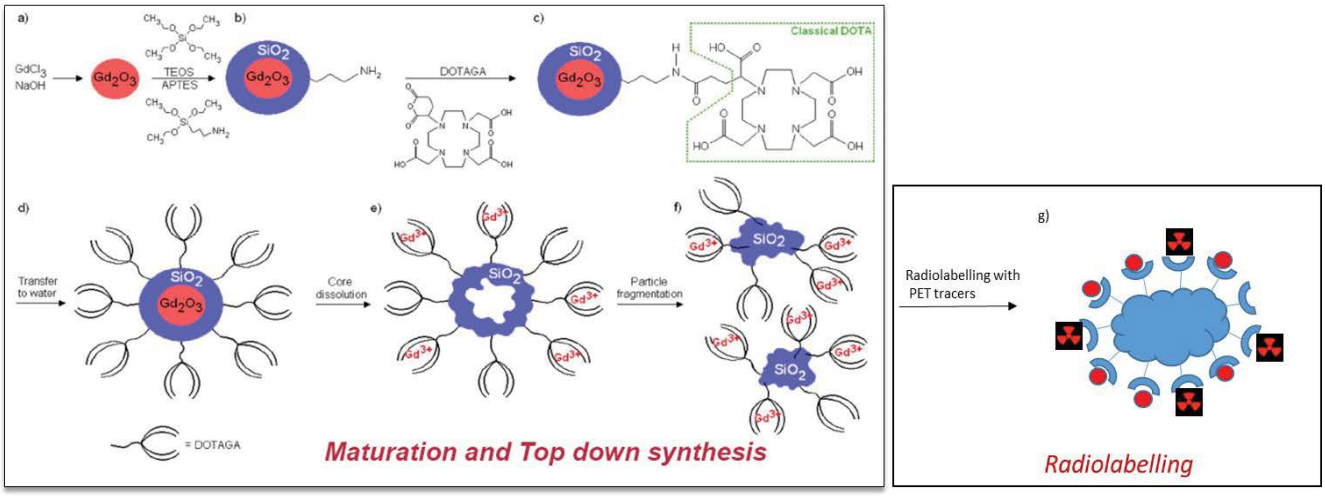

Figure 1: Preparation of AGuIX: (a-c) DOTAGA grafting, (d) transfer to water and addition of DTPA, (e-f) core dissolution and polysiloxane fragmentation and (g) radiolabeling with PET tracers.

tion is thus effectively increased up to days. Scandium is generally considered to be chemically like lanthanides in which the coordination chemistry is well established, especially for nuclear medicine [25].

Finally, Ga radioisotopes used in nuclear medicine are ^{68}Ga and ^{67}Ga. The γ energies for ^{67}Ga (Eγ = 173 keV (89%) and 247 keV (95%)) are useful for SPECT imaging [26], whereas the β^+ energies for 68Ga (E_β = 829.5 keV (1.2%) and 1899 keV (87.9%)) are suitable for PET. But, in the process of optimizing radiolabeling process, 67Ga is more convenient since its half-life of 3.2 days is much longer than the half-life of 68Ga ($T_{1/2}$ = 1.12 h).

The aim of this work was to develop and optimize the radiolabeling of different GBN batches (different grafted DOTA percentage) with ^{64}Cu, ^{67}Ga and ^{44}Sc (Figure 1). Labeling parameters evaluated were molar ratio, reaction pH and temperature. The effect of radiolabeling on GBN size and distribution was checked.

Materials and Methods

Chemicals and reagents

Analytical grade (MeOH, EtOH, conc. aq. HCl, HNO_3, conc. aq. ammonia, ammonium acetate) or pure reagent grade (all other chemicals) reagents are commercially available. They were used as received unless otherwise specified. Deionized water (18.2 MΩ cm^{-1}; Milli-Q, Millipore) was used throughout the work. Commercially available 1,4,7,10-tetraazacyclododecane-1,4,7,10-tetraacetic acid (DOTA, CheMatech, France) was used as received. Ammonium acetate (99.9%) was purchased from Fisher Scientific (New Jersey, USA or Saint Quentin Fallavier, France). Optima® grade nitric and hydrochloric acid (HNO_3, HCl) were purchased from Fisher Scientific (France) and used without further purification. TLC silica gel 60 plastic sheets (MKC18F Silica Gel 60Å, layer thickness of 200 µm) were obtained from Merck GaA (Darmstadt, Germany). Chemical grade methanol was purchased from Fluka (Switzerland). BSA (Uptima Interchim #UP36859A Batch R06L379) was diluted to 2 g/L.

Table 1: Different batches of NPs that have been synthesized and used in this work with their main characteristics (radii are extracted after synthesis from DLS measurements given in number).

Name	Ligand nature and content	Radiii (nm)
AGuIX@DOTA2%	2% free DOTA 1	1.8
AGuIX@DOTA9%	9% free DOTA	1.3
AGuIX@DOTA37%	37% free DOTA	2.0
AGuIX@DOTA60%	60% free DOTA	2.5

Nanoparticles

Ultrasmall Gd based nanoparticles (GBN) were obtained from Nano-H Company (Lyon, France). The main characteristics provided by the company on the different batches are summarized in Table 1. Their synthesis has been described elsewhere [8]. Regular AGuIX are composed of DOTA ligand, and 97-99% of them complexed with Gd^{3+} ions. However, these particles can be modified to increase the number of free DOTA. In this work, we worked with 4 different batches designed as AGuIX@DOTA2%, AGuIX@DOTA9%, AGuIX@DOTA37% and AGuIX@DOTA60% presenting respectively 2%, 9%, 37% and 60% free DOTA chelates at the surface available for radiolabeling (Table 1).

Radionuclides

The nuclear characteristics of the radionuclides (emissions and energies) are summarized in Table 2. ^{67}Ga was purchased from Cis Bio International (France) in the citrate form with a total activity of 173 MBq/mL. The batch was diluted to 5 mL by using aq. HNO_3 (1% w/w) prior to its use and is referred to as the ^{67}Ga stock solution. An aliquot of 150 µl was taken for metal concentration determination. To this aim, an ICP-OES (ThermoFischer ICAP 6500 DUO ICP-AES) was used, various metals were analyzed (Al, Ca, Cu, Co, Cr, Fe, Mn, Mg, Mo, Na, Sc, Ni and Zn).

Table 2: Main nuclear characteristics of radionuclides [27].

Isotope	Radioactive Half-life	Production route used	γ-energy (keV) and intensity (%)
Cu-64	12.7 h	Ni-64 (d,n) Cu-64	1345.84 (0.473).8
Sc-44	3.9 d	Ca-44 (p,n) Sc-44	1157.031 (99.9) 93.311 (39.2)
Ga-67	3.3 d	Zn (2n,p) Ga-67	184.577 (21.2) 300.219 (16.80)

For each element, the wavelength was selected to reach the higher relative emissions and was the one with the least interference from other signals. The ICP-AES was calibrated using commercially available single- and multi-element standards (~10 ppm, SCP Science) in dilute nitric acid (1% w/w). The batches to be analyzed were in acidic solutions. Before analysis, they were collected and diluted in aq. HNO_3 (1% w/w). Only Al has been identified as a main stable contaminant. Its concentration in the stock solution was approx. 1.15×10^{-4} mol/L. The resulting specific activity was low at 40.7 Ci/g.

The procedure of $^{44m}Sc/^{44}Sc$ production at Arronax cyclotron (France) was described elsewhere [19]. Briefly, an enriched $CaCO_3$ (500 mg) target irradiated for 3h with a 16.4 MeV deuteron beam of ≈ 300 nA intensity, was dissolved in aq. HCl (4 M, 10 mL) and the solution was loaded onto a DGA column (Triskem, France). Next, the column was conditioned with aq. HNO3 (1 M, 10 mL) to eliminate metallic impurities. Finally, ^{44}Sc was eluted with 400 µL of aq. HCl (0.1 M). The solution was evaporated to dryness and re-dissolved in HCl solution (0.1 M) to get ^{44}Sc(III) chloride hydrate with a resulting activity > 100 MBq in 400 µL ($^{44m}Sc/^{44}Sc$ activity ratio equal to 2% at the end of the chemistry step, around 4 hours after EOB). The final solution of $^{44m}Sc/^{44}Sc$ was counted on a γ-spectrometer (Ortec-Ametek, France). The energy rays used for identification were 271.1 keV and 1157 keV for ^{44m}Sc and ^{44}Sc respectively, with a branching ratio of 98.8% and 99.9% (Table 2). After the purification, the expensive target material was re-covered for reprocessing. This $^{44m/44}Sc$ solution was diluted to 1.5 mL with aq. HNO_3 (1% w/w) prior to its use and corresponds to the ^{44}Sc stock solution. The ICP-OES analysis identified the following main stable contaminants (Al, Fe, Ni and Zn) with a total metal concentration of 1.1×10^{-5} mol/L. The resulting specific activity is thus 3484 Ci/g.

The deuteron production route is also used for ^{64}Cu production on the Arronax cyclotron (France). A highly enriched ^{64}Ni target was electroplated on a gold disk (99.99% purity). The purification procedure uses HBr on AG1X8 chromatographic column. After the production procedure, the enriched material was recovered with a yield of 95% [28] for further reprocessing. A deuteron beam at 16 MeV was used for irradiation with 50 µA current impinging on a 10 µm thick target for 150 minutes. Copper-64 was recovered as $CuCl_2$ with a high radio isotopic purity (> 99.90%). The total activity for ^{64}Cu was 102 MBq in 50 µL. This solution was diluted to 1.5 mL with aq. HNO_3 (1% w/w) prior to its use and corresponds to the ^{64}Cu stock solution. Main contaminants identified by ICP-OES, were Cu, Fe and Ni, with a total metal concentration of 1.2×10^{-4} mol/L. The resulting specific activity was 42346 Ci/g. This specific activity was lower than the one published by Mc Carthy, et al. (i.e.94-310 mCi/µgram Cu) but was sufficient for radiolabeling [29].

HF-MALS experimental set-up and method

HF5 analyses were performed using an Agilent Infinity1260 HPLC system (Agilent Technologies, Santa Clara, CA, USA) consisting of a degasser, an isocratic pump, an autosampler (HiP BioLS HP 1260, Agilent technologies), a variable wavelength UV detector (MWD RL, Agilent technologies combined with an Eclipse® DUALTEC separation system (Wyatt Technology Europe, Dernbach, Germany).

The HF5 channel (Wyatt Technology Europe) consisted of two sets of ferrules, gaskets and cap nuts used to seal a polymeric hollow fiber inside a plastic cartridge. The scheme of the HF5 cartridge, its assembly and the modes of operation of the Eclipse® DUALTEC system have already been described elsewhere [20]. The hollow fiber was a polyether-sulfone (PES) fiber, type FUS 0181 available from Microdyn-Nadir (Wiesbaden, Germany) with the following characteristics: 0.8 mm ID, 1.3 mm OD, and 10 kDa Mw cut-off, corresponding to an average pore diameter of 5 nm. The HF5 channels used in the experiment were a standard cartridge containing a 17 cm long fiber.

The OpenLab CDS ChemStation (Agilent Technologies) data system for Agilent instrumentation allows the control of the instrumentation and analytical analysis. The software package Wyatt Eclipse @ ChemStation (Wyatt Technology Europe) was used to set and control the flow rate and to move the focus position during the sample focus/concentration.

An 18-angle multiangle light scattering detector model DAWNMD HELEOS (Wyatt Technology Corporation, Santa Barbara, CA, USA) operating at a wavelength of 658 nm, was used to measure the radius of particles in solution. A RID 1260 (Agilent technologies) differential refractive index (dRI) detector operating at a wavelength of 280 nm was used on occasion as a concentration detector, when the capabilities of the UV detector were overcome by the complexity of

Table 3: Flow conditions for HF5 analyses.

Start time (min)	End time (min)	Duration (min)	Mode	Vc (ml/min)	Vx start (ml/min)	Vx start (ml/min)
0	1	1	elution	1	0	0
1	2	1	focus	1	0.5	0.5
2	7	5	Focus + inject	1	0.5	0.5
7	19	12	elution	1	0.65	0.65
19	20	1	Elution	1	0.65	0.05
20	25	5	Elution + inject	1	0.05	0.05
25	28	3	Elution	1	0	0
28	30	2	Elution + inject	1	0	0

the sample. ASTRA® software version 5.3.2.14 (Wyatt Technology Corporation) was used to handle signals from the detectors (MALS, dRI and UV) and to compute the protein Mw and concentration values.

An HF5 method is composed of the following steps: focus, focus-injection, elution and elution-injection. During focus the mobile phase is split into two different streams entering from the fiber's inlet and outlet; during focus-injection, the flow settings are the same as those described in the focus step when the sample is introduced into the channel through the inlet and focalized in a narrow region. Then, in the elution step, the flow of mobile phase enters the channel inlet and part of it comes out transversely (cross-flow); lastly, during elution-injection, no cross-flow is applied (the flow is not split anymore), allowing for any remaining sample inside the channel to be released; also, the flow is re-directed in the injection line as well to clean it before the next injection.

The flow conditions for the different HF5 analysis are shown in Table 3. Longitudinal flow is indicated as Vc, while cross/focus flow as Vx. In flow-injection analyses (FIA) neither focus nor cross-flow are applied, thus allowing all injected analytes to exit from the channel without retention. The solvent used is Ultrapure water that is filtered at 0.45 µm and 0.1 µm on Durapore filters (Millipore) before injection into the HF5 system.

A stock suspension at 10 mg/ml in ultrapure water was prepared. For each suspension, 2 injections were performed 10 µL and 20 µL leading to a final injected concentration of 100 µg/mL and 200 µg/mL respectively.

Radiolabeling

Labeling of AGuIX@DOTA with M^{x+} radioisotopes was performed by mixing a GBN stock suspension in acetate buffer (0.1 M) with a certain amount of M^{x+}. In all the following sections, we will refer to radioisotope molar amount (noted M) to be the sum of the radioisotope concentration and all the metallic impurities that have been measured by IPC-OES in the initial batch, corrected by the dilution factor in the radiolabeling experiment. Since DOTA ligand is not selective for a given metal, all metallic species in solution could compete for the complexation. Several parameters were meticulously studied for the optimization of the radiolabeling in repeated experiments (at least in triplicate): pH of the reaction mixtures and the ligand concentration (precisely, ligand molar excess over radioisotope molar amount). No attempt was made to play with the temperature since, in contrast to antibodies, these nanoparticles can withstand high temperatures. The solutions were then heated at 90 °C up to 60 min in a sand bath. To determine effect of pH on the M^{x+}-GBN complex formation, different buffers were used: acetate buffers (C = 0.1 M; pH = 4 or 5.5) or an MES buffer (pH = 7, 0.1 mol/L). Before and after the heating step, pH was measured at room temperature (pH electrode was calibrated using three commercial standards) with no significant changes observed.

Thin layer chromatography (TLC) was used to determine radiochemical yield for all metal complexes. At 1 cm from the origin of a 2.5 by 7.5 cm TLC silica gel plate, 1 µL of the sample was spotted. Citrate buffer (0.25 mol/L; pH = 5.2) was used as the eluent for ^{67}Ga and ^{44}Sc-radiolabeling experiments whereas a citrate buffer was used at 0.2 mol/L (pH = 5.2) for ^{64}Cu experiments. These eluents were optimized as a function of the cationic chemistry of the radionuclides used. The metal cation remains at the origin while the M^{x+}-NPs complex moves with the solvent on the silica surface under these conditions. The strips were read on a Cyclone-Perkin detector (Perkin Elmer, France) to determine radiolabeling yields.

Results and Discussion

First, we developed a HF5method in aqueous media for the size-fractionation of AguiX NPs. These NPs were detected with satisfactory sensitivity, the method has been shown to be robust and reproducible [30].

HF-MALS on AGuiX®

HF5 allowed sample separation using water as the mobile phase. Thus, samples were analyzed in their native formulation, limiting potential modification due to fractionation conditions. The HF5-MALS flow conditions are described in Section 2.4. The AGuiX NPs analysis is reported in Figure 2. A void peak is observed at 7.5 min for the unretained species (such as unreacted reagents for sample preparation or small species dimension-ally comparable to channel membrane cut-off). The retention peak is observed for a tR = 9.88 min typical for the nanostructure. A hydrodynamic radius of about 3.5 nm was determined for the NPs. It was not

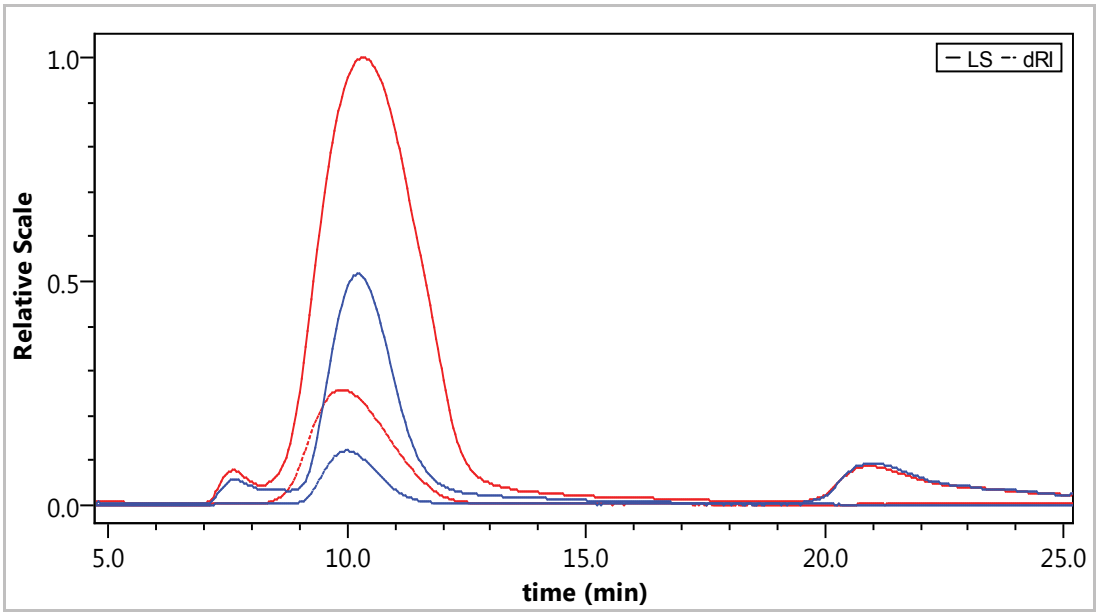

Figure 2: AGuIX@DOTA2%, nanoparticles analyzed by HF5-MALS in water. Light scattering (LS) signal at 90 °C (line) and refractometer signal (dRI dashed line). The two colors represent two concentrations of the same sample, respectively 100 µg/mL (blue line) and 200 µg/mL (red line).

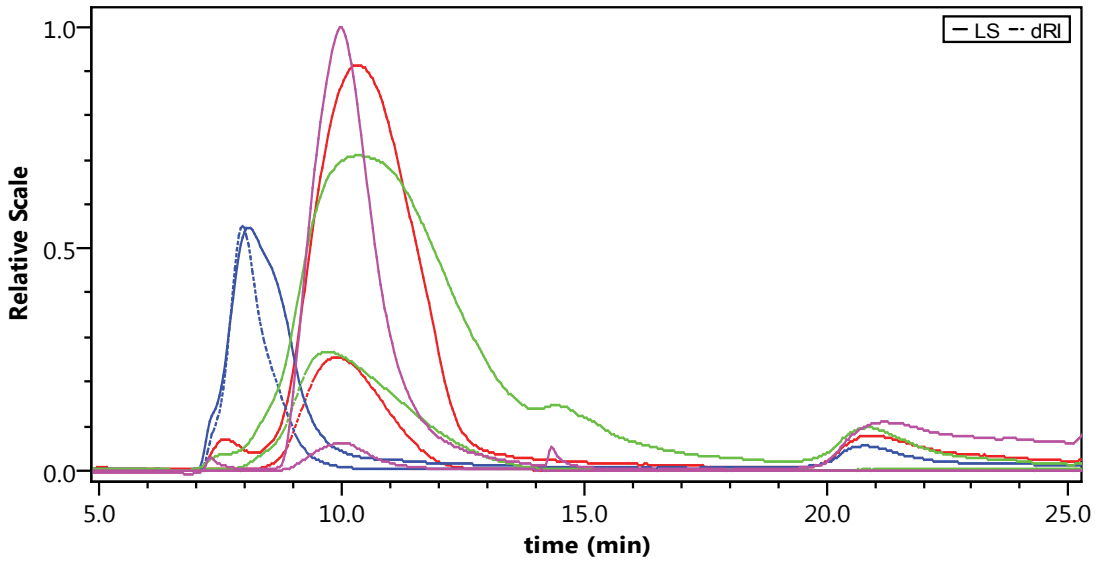

Figure 3: Comparison of LS and RI chromatograms for AGuiX@DOTA2% (red), AGuiX@DOTA9% (blue) AGuiX@DOTA60% (green) and BSA (pink).

possible to have access to the *rms* value and thus the *rg/rh* ratio for determining the exact conformation. It is assumed in the following that nanoparticles are spherical.

It is also possible to observe that at the end of elution (t_R = 20 min) during the elution injection step, a small light scattering (LS) signal is apparent meaning that all eluted samples are separated during the HF5 analysis. Due to the presence of a small LS signal and a non-significant RI signal (data not shown), it means that no NPs species are released at the end of the elution. Usually, for a monodisperse sample, its average radius is not related to the averaging method used; its polydispersity will equal 1. By contrast, in the case of polydisperse samples, containing a mixture of species, the polydispersity will differ from 1. In the case of AGuiX NPs, the calculated polydispersity from the HF5-MALS experiments was found to be 1.002, indicating that the nanoparticles are highly monodispersed.

The recovery of the samples analyzed was quite low (i.e. approx. 15%) even after cross-flow release. The assumption is that only PES at 10 kDa for the cut-off exists for the hollow fiber. Since these nanoparticles are ultra-small, a most suitable cut-off would be probably 5 kDa, and even 1 kDa to improve the recovery. Those cut-off thresholds do not exist for hollow fiber and it will certainly consist in a future development that would be required from HF5 supplier, especially in the field of nanomedicine.

Despite this fact, the fractionation and size charac-

terization of AGuiX nanoparticles at low concentration (10 mg/mL, injected volume 20 µL i.e. injected weight 200 µg) in water was shown to be reproducible by HF5.

Only AGuiX@DOTA2%; AGuiX@DOTA9% and AGuiX@DOTA60% were analyzed by HF5. For these 3 samples, triplicate injections were performed, and we obtained good re-producibility on the retention time for each sample. Typically, retention times were found to be t_R = 9.88 min, t_R = 9.95 min, t_R = 9.65 min for AGuiX@DOTA2%; AGuiX@DOTA9% and AGuiX@DOTA60% respectively. The elution profiles of these 3 samples are summarized in Figure 3. Regardless of the percentage of DOTA grafted at the surface, elution profiles were similar with very close retention times. An exception is for AGuiX@DOTA60% which is more heterogeneous since a peak is observed at t_R = 15 min that corresponds to aggregates and/or particles of larger sizes. BSA was used as an external standard for size calibration with a well-known size of 3.5 nm. As noted in Figure 2, AGuiX@DOTA2% and AGuiX@DOTA60% have similar retention times as BSA meaning their sizes are of the same order of magnitude. For AGuiX@DOTA9% the earlier retention time compared to the two other nanoparticles means that its size is smaller than BSA (i.e. 3.5 nm) and AGuiX@DOTA9% are not sufficiently retained by the hollow fiber due to their smaller size.

Radiolabeling

When performing radiolabeling on a polymeric or a nanodimensional system, two different pathways could be used. In the first pathway, the polymer/particle and the label are bound through a synthetic step. It is called pre-radiolabeling. In the second pathway, one compound (in the case of metals this is a bifunctional chelate) is labeled first and subsequently the polymer/particle is formed. It is so called post-radiolabeling. Pre or post-radiolabeling depend on several factors, above all the half-life of the chosen radionuclide. Most of the published labeling procedures belong to the second category (i.e. post-radiolabeling) First, the polymeric or nano-particular system is formed, then a chelate is grafted to this system and finally the radionuclide is introduced. In the present work, this procedure was applied to various AGuiX NPs. The same type of NPs has previously been labelled with different radioactive isotopes either directly with DOTA ligands present at the surface of the nanoparticles (^{111}In) [2] or after grafting of a different ligand (^{68}Ga [31] and ^{89}Zr [32]). The chelation of Zr(IV), is usually performed via DFO chelates, although no chelation constant is available [33]. In(III) is known to be well chelated by DOTA, with a thermodynamic constant close to that of NOTA (log K_{DOTA} = 23.9 vs log K_{NOTA} = 26.2) [34] (Table 4). After labelling with In(III), an interesting pattern of biodistribution of radiolabeled NPs is observed after intravenous injection in mice with an exclusive renal elimination (quantity of 111In < 0.2% of the injected dose in organs other than the kidneys (29.8 ± 6.8% ID) and bladder (57.9 ± 27.4% ID) 3 hours after intravenous injection of the NPs) [2] and a passive accumulation by EPR effect in tumors [1]. In comparison, for the chelation of Ga(III), NOTA is more appropriate than DOTA (log K_{DOTA} = 21.3 vs. log KNOTA = 31.0) [35]. The addition of new chelates at the surface of the nanoparticle is of interest to optimize the radiolabeling for PET/MRI multimodal imaging, but to obtain a quantitative biodistribution of the AGuIX NPs available for clinical applications with no change of the structure of the nanoparticle synthesized in compliance with Good Manufacturing Practices (cGMP) conditions, an optimization of the radiolabeling with DOTA chelates is of great interest. To do such optimization, different parameters like pH or molar ratios should be tested for the radiolabeling of the AGuIX with scandium, copper and gallium isotopes.

Determination of optimum pH: The pH determination for all metals was done with AGuIX@DOTA2% nanoparticles and AGuIX@DOTA60% because these batches offered the minimum and maximum amount of free DOTA (2 and 60% respectively) at the surface available for complexation with PET tracers. These experiments were performed at 90 °C for 60 minutes. For sake of clarity, only results on AGuIX@DOTA2% for 44Sc for 3 M:L ratios (i.e. 1:10; 1:100; 1:1000) are presented in Figure 4.

The radiolabeling yield was between 45 and 65% in each case. The radiolabeling yields reached for ^{64}Cu and ^{67}Ga are higher (almost 100%) except for M : L =1:10 ratio with ^{67}Ga for which yields are about 40% at pH 4. Scandium and Gallium are trivalent elements and their ionic radii are not so different; one would expect to reach the same radiolabeling yields for both elements. The observed differences could thus be explained by the specific activity of the initial batch of gallium, which was lower than for scandium.

For AGuIX@DOTA60%, with a higher percentage of free DOTA, results are presented in Table 5 for the three radionuclides. From these results (Figure 4 and Table 5), it can be seen that the pH does not influence

Table 4: Complexation constants obtained between the metallic element and DOTA ligand [25,35].

Metal	Complexation Constant
Cu	22.72
Sc	30.79
Ga	21.33

Table 5: ^{67}Ga, ^{64}Cu and ^{44}Sc: labeling yields for AGuIX@DOTA60%; Labeling conditions were 1:100 molar ratio, 0.1 M ammonium acetate buffer, 90 °C, 60 min, n = 3. Values are given with 5% uncertainty.

pH	^{67}Ga	^{64}Cu	^{44}Sc
4	62.1	100	96.7
5	62.5	100	97.0
6	62.5	100	97.8
7	62.5	100	97.4

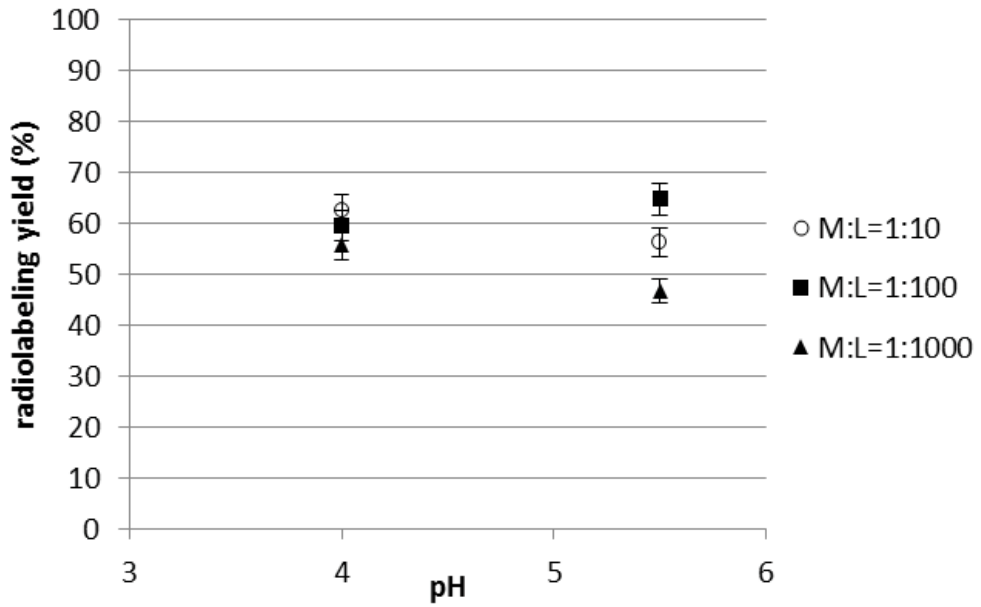

Figure 4: Evolution of the radiolabeling yields for AGuIX@DOTA2% as a function of pH for ^{44}Sc.

significantly the radiolabeling efficiency for this range. For the following, it was decided to fix the pH at 4 for studying the influence of other parameters. It can be seen with this last study that the radiolabeling yield obtained with 44Sc for AGuIX@DOTA60% is higher than for AGuIX@DOTA2% (respectively around 97% and 60%). It highlights that it is important to be able to optimize the nanoparticle structure to improve radiolabeling for the isotope of interest.

Time monitoring: Radiolabeling was monitored with time for the different batches of nanoparticles and for the three radionuclides of interest results are presented in Figure 5. The maximum radiolabeling yields of these AGuiX NPs were attained after 60 min for scandium-44, which is quite long for DOTA radiolabeling, as scandium is generally considered to be chemically like lanthanides whose coordination chemistry is very well established. DOTA labeling with lanthanides is usually done at 80 °C for 153Sm and 100 °C for 177Lu. ^{153}Sm-DOTA optimum temperature is reported at 70 °C with pH 5 for 40 minutes by Hu [36]. Additionally, Stimmel [37] reported a maximal temperature at 22 °C, at pH of 6 after 2 h of contact. Described γ-Fe_3O_4 and cerium ammonium nitrate inorganic NPs were described by Locatelli, et al. [38]. Their radiolabeling yields at 23 °C did not reach more than 90%. For DOTA-^{44}Sc, it was published that the most suitable conditions are reached for a metal-to-ligand ratio of 1:3 in acetate buffer at pH = 4, after heating at 70 °C for 20 minutes. These conditions provide the best labeling yields > 95% [25,27,39]. These values were in agreement with previous studies performed on ^{44}Sc-DOTATOC and ^{44}Sc-DOTATATE, when the isotope was eluted from a ^{44}Ti/^{44}Sc generator [40,41]. The specific activity was not the major parameter for radiolabeling by DOTA as highlighted by the majority of the studies but would be of major importance for further use with biological vectors. The specific activity will be assessed by varying the metal-to-free ligand ratio at the surface of the nanoparticle in the corresponding section.

Among the different chelating agents used for gallium, DOTA (frequently used also for copper or scandium), but also NOTA are potent chelators for the smaller gallium(III)-cation. So far, only NOTA and its derivatives have been used to radiolabel nanodimensional systems (i.e. organic and inorganic) with ^{68}Ga [31]. ^{67}Ga radiolabeling was monitored as a function of time at pH = 4, and for molar ratios ranging from 1:10 to 1:1000. It was showed that the best yields were reached for 30 minutes for the 1:10 molar ratio and this time could be reduced to 15 minutes for the highest metal-to-ligand ratio. Yields ranging between 10 ± 5% and 100 ± 5% were obtained depending upon the metal- to-ligand ratio used. 68Ga radiolabeling performed with NOTA or DOTA resulted in high radiolabeling efficiency after 10 min at RT and, specific activities with 68Ga were as high as 9.8 mCi/nmol (i.e. 362 GBq/nmol) without purification [42].

^{64}Cu is a radiometal that requires a bifunctional chelator for stable attachment to bio-molecules. DOTA or its derivatives are the most popular ones. DOTA was originally considered for lanthanides (e.g., Gd^{3+}), but has been used for a wide range of (radio)metals as well. Since DOTA has four carboxylic functional groups on the side-chains of the macrocycle bearing four nitrogens, complexation of the Cu^{2+} ion leads to a deformed octahedral structure, which is preferred due to the Jahn-Teller effect thereby leaving two of the acidic functions free. One acidic function is available for coupling to NPs and the second one allows further derivatization or acts as an additional hydrophilic group. Other macrocyclic chelates are TETA (1,4,8,11-tetraazacyclotetradecane-N,N',N'',N'''-tetraacetic acid) and NOTA or derivatives of these. In

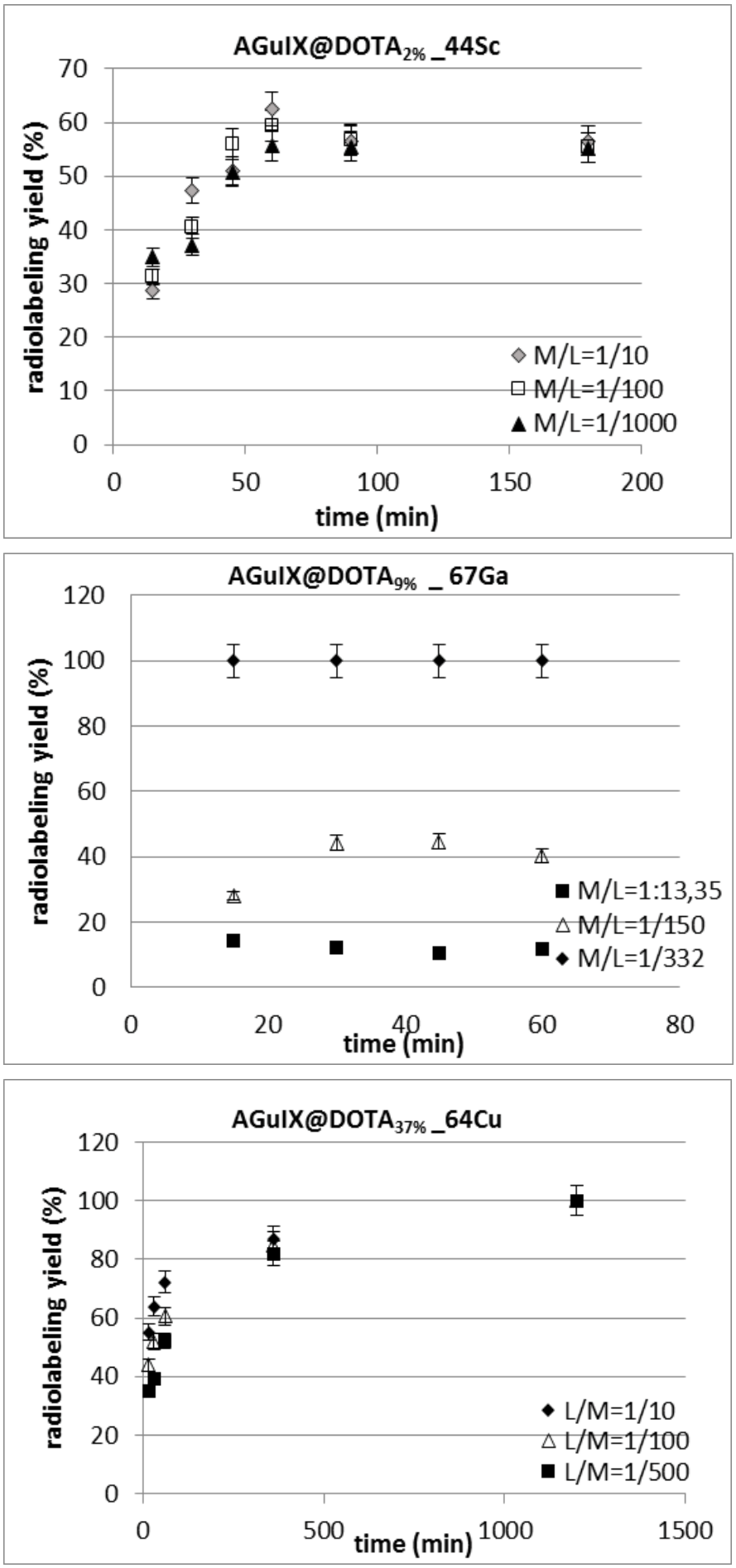

Figure 5: Radiolabeling yields with time for various M/L ratio at pH = 4, for (A) AGuIX@DOTA2% nanoparticles (1.5% of free DOTA) with ^{44}Sc; (B) AGuIX@DOTA9% (9% of free DOTA) nanoparticles with ^{67}Ga and (C) AGuIX@DOTA37% (37% of free DOTA) with ^{64}Cu.

the case of 64Cu, the maximum labeling yield is usually reached between 23 °C to 37 °C, which is the range reported for ^{64}Cu -DOTA labeling conditions in literature [43-45]. At 90 °C, the radiolabeling reached 100% after 15 minutes, for all the nanoparticles considered in the present work. This is higher than the radiolabeling yields previously obtained for the corresponding ultra-small AGuIX-NOTA nanoparticles with ^{64}Cu and ^{68}Ga that were 81-85% [46], that may be explained by the kinetics of complexation of copper with DOTA that is faster than with NOTA. In an acetate buffer at pH 4, it was shown that radiolabeling was stable out to 24 h.

The results of ^{64}Cu radiolabeling with time are presented in Figure 4C for AGuIX@DOTA37% only. For pH 4, 100% of radiolabeling was obtained for all the nano-particles considered in this work after 1 day. From literature data, the case reported were on [^{64}Cu] CuS nanoparticles that have been prepared by metathesis reaction of $^{64}CuCl_2$, $CuCl_2$, and Na_2S at 95 °C for 1 h [47]. Co-heating of $^{64}CuCl_2$, gold chloride, and copper acetylacetonate in oleylamine at 160 °C for 2 h produced 10 nm [^{64}Cu] Au NPs [48]. The other case reported concerns the production of [^{64}Cu] Fe_3O_4 NPs by microwave-assisted heating and via hydrolysis of $^{64}CuCl_2$, $FeCl_2$, and $FeCl_3$ [49]. The chemical reactivity of ^{64}Cu is recognized to be relatively low. Thus, the synthesis of [^{64}Cu]-NPs usually requires high temperatures and longer incubation time, that increases the risk of radiation contamination. Briefly, for inorganic nanoparticles composed of either iron oxide or silicone, with DOTA as chelating moiety, the radiolabeling of ^{64}Cu was performed for 1 h at temperatures ranging from 37 to 40 °C and at a pH range of 5.5 to 6.5. Yang, et al. [50] showed that the radiolabeling yield was 94% whereas Glaus, et al. [51] obtained yields ≥ 95%. In that case, they reached specific activities of 2-4 GBq/mmol.

Determination of the molar ratio: The optimum conditions for M^{3+} are achieved when a high radiochemical yield (over 95%) is obtained. This yield was selected according to the most common desirable yield reported in literature [32,34] to eliminate the purification step after radiolabeling. Because M^{3+}-DOTA labels at 23 °C, at pH 5-7 and is stable *in vitro* and *in vivo* when labeling under these conditions, it is expected to label M^{3+} -AGuIX@DOTA in high yields (over 95%) [16,45]. The radiochemical yield was evaluated by TLC as described above.

Determination of optimum conditions for each isotope was completed and the specific activity assessed. To determine the optimum molar ratio of ^{67}Ga: AGuIX@DOTA the pH was adjusted to 4 with acetate buffer and the solution was heated for 60 minutes at 90 °C. Results are presented in Figure 6A. Surprisingly, to reach high radiochemical yield, the metal-to-ligand ratio seems not to be the most important parameter for a fixed number of free DOTA at the surface. By increasing the number of free DOTA available at the surface of the nanoparticles, one would expect to increase the radiolabeling yields; which was not the case. From the thermodynamic point of view, if the number of DOTA increases, the equilibrium is displaced to higher complex formation; except if a steric hindrance of the ligand occurs leading to lower complex formation, which seems to be the case. For AGuIX@DOTA2% (i.e. 2% of free DOTA), 1:150 metal to ligand ratio was necessary to attain 100% radiolabeling which corresponds to 2.9 nmol of DOTA. For AGuIX@DOTA9% and AGuIX@DOTA37%, these ratios were respectively 1:332 (i.e. 5.75 nmol) and 1:665 (i.e. 11.5 nmol). In 2011, ^{18}F-labeled rare earth containing NPs were developed by Liu, et al. [52] These authors [52] used $NaYF_4$ for doing the surface-modification of their particles with Gd^{3+} by cation exchange with Y^{3+} for their use in MRI or in luminescence studies with different rare earth elements (Yb, Er). Radio-TLC indicated an excellent labeling yield of 92% (after 40 min of reaction time at 90 °C).

These optimum metal-to-ligand ratios obtained on AGuIX or functionalized AGuIX particles lead us to evaluate the resulting specific activity reachable for each nanoparticle. The measure of the radioactivity per unit mass of the compound is the specific activity; the higher the specific activity of a radionuclide, the higher both the percentage of radioactive atoms and the deliverable dose are. Specific activity may or may not be important depending on the number of sites available for targeting. For instance, bone is considered a large capacity site and does not require radioisotopes with high specific activity. Low specific activity radioisotopes such as 153Sm in Quadramet® and ^{166}Ho in the Skeletal Targeted Radiotherapy agent have been used for pain palliation and bone marrow ablation, respectively [53]. Low capacity sites such as receptor sites, which are present in low numbers, require high specific activity radioisotopes. The achievable specific activities are 8.0 ± 0.2 µCi/nmol for AGuIX@DOTA2%., 4.0 ± 0.2 µCi/nmol for AGuIX@DOTA9% and 2.0 ± 0.2 µCi/nmol for AGuIX@DOTA37%. These values are quite low by comparison to published values of 500 Ci/nmol [54].

The most surprising result was obtained for AGuIX@DOTA60% which exhibits the highest percentage of free DOTA at the surface, available for complexation. One would expect to reach 100% for low metal to ligand ratio, while only 54% of radiolabeling yield was reached after 60 min. Longer reaction times did not improve the yield and even led to some degradation of NPs. No attempt to proceed with further purification was done in this work.

The radiolabeling results regarding the coordination chemistry of the radiometal is shown in Table 4. From published data, DOTA is not the most suitable ligand for coordinating Ga. NOTA is usually the most suitable chelate for Ga. Even though both ligands exhibit high

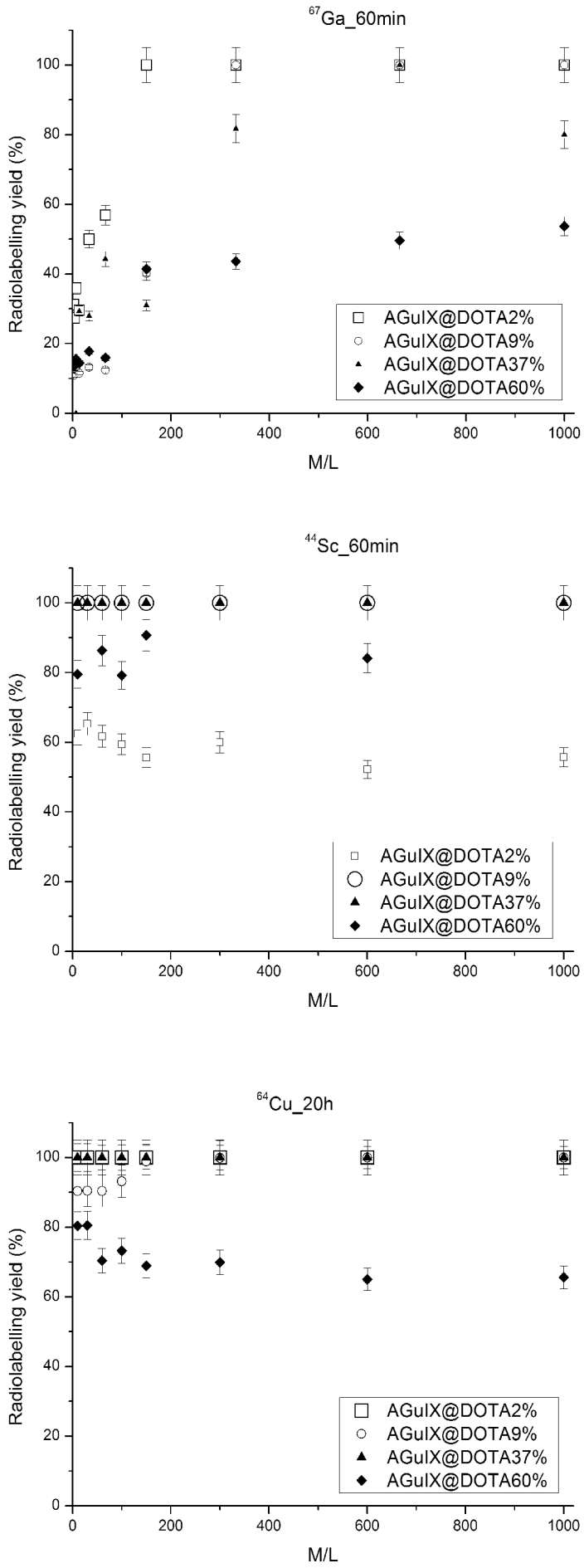

Figure 6: Evolution of the radiolabeling yields (n = 3) as a function of time for various M/L ratio at pH = 4 for AGuIX@DOTA2% (1.5% of free DOTA), AGuIX@DOTA9% (9% of free DOTA), AGuIX@DOTA37% (37% of free DOTA) and AGuIX@DOTA60% (60% of free DOTA) nanoparticles (A) with ^{67}Ga; (B) with ^{44}Sc and (C) with ^{64}Cu.

stability constants (log K > 20), the NODA-Ga constant is found to be 31.0 whereas it is 21.3 for the DOTA-Ga system. In this work, DOTA was used as the ligand but by changing the ligand (for instance NOTA), improved 67Ga radiolabeling yields may be achieved as was published for ^{68}Ga [32] (Table 4).

Results with ^{44}Sc are presented in Figure 6B. For AGuIX@DOTA9% and AGuIX@DOTA37%, the increment in ^{44}Sc did not result in big differences in yields at the chosen molar ratios (1:10 to 1:1000). Radiolabeling was 100% at all molar ratios. The highest resulting specific activity was determined for metal-to-ligand ratio of 1:10 (i.e. 1.2 nmol of ligand) and was calculated to be 13.7 ± 0.5 µCi/nmol. This difference in the resulting specific activity compared to ^{67}Ga could be explained by the initial specific activity of the radionuclide batch which was 87-fold higher in the case of ^{44}Sc compared to ^{67}Ga (section 2.5).

For AGuIX@DOTA2%, the maximum yield obtained was 60%. By increasing the number of free DOTA (up to 60% in AGuIX@DOTA60%), the radiolabeling yield slightly increased to 85% which highlights the importance of structure optimization to improve radiolabeling yield. Regarding coordination chemistry of this radiometal, DOTA is the most suitable ligand for scandium [55]. This probably means that, in contrast to the Sc-DOTA system, the theoretical free DOTA were not totally available for radiolabeling. Additionally, to this, for AGuIX@DOTA60%, the higher number of free DOTA may lead to a less accurate determination of the free ligands by comparison to the other nanoparticles studied in the present work.

The same approach was used on other types of hybrid nanoparticles. Mesoporous silica NPs were labeled by Huang, et al. [56] with Gd^{3+} (T1-contrast agent in MRI) together with $^{64}Cu^{2+}$ (a PET radiotracer). Similarly, DOTA was employed by these authors as a chelating agent since copper and gadolinium could be inserted into the surface pores. Their labeling conditions were 1 h at a pH of 5.5 and 40 °C leading to > 98% of radio-labeling. This has been shown to allow a highly stable radiotracer, which exhibits high uptake in the sentinel lymph node.

The increment in ^{64}Cu: AGuIX@DOTA did not result in big differences in yields in the chosen molar ratios (1:10 to 1:1000) as seen in Figure 6C. The maximum yield was obtained at 1:10 with 100 ± 5% of the labeled compound for AGuIX@DOTA2% and AGuIX@DOTA37% at 1:150. These molar ratios seem high; though there is no reference to the optimum molar ratio used in the reviewed literature. Quantum dots (QDs) were developed and some groups have coated manganese-doped silicon QDs with dextran Tu, et al. [57]. These QDs were then coupled to a DO3A-derivative for chelating ^{64}Cu. The radiolabeling was performed in acetate buffer (pH 5.5), followed by an EDTA-competition and a radiolabeling yield of 78% was obtained.

The minimum yield was obtained for AGuIX@DOTA60%, as previously observed with the other radionuclides since at 1: 10, 80 ± 5% of radiolabeling was reached. Even lower yields were observed by increasing the ligand-to-metal ratio. As already discussed previously, the theoretical free DOTA were not totally available for radiolabeling. For AGuIX@DOTA60%, the higher number of free DOTA may lead to a less accurate determination of the free ligands by comparison to the other nanoparticles studied in the pre-sent work. Other bifunctional Chelators should be considered for improving radiolabeling with ^{64}Cu. As recently published by Lee, et al. [58], click chemistry could be applied to attach a 64Cu-radiolabeled alkyne complex to azide-functionalized glycol chitosan nanoparticles *in vivo*. The radiolabeling procedure was performed within 30 min at 40 °C, in which a DOTA-DBCO-conjugate was labeled in 98% yield.

For all ^{44}Sc- radiolabeled NPs, HF5 analysis were performed again in the same conditions than the ones described in section 2.4. Same profiles (not shown here) were obtained compared to the native AguiX nanoparticles, indicating the integrity of these nanoparticles when radiolabeled.

Conclusions

Gd-based AGuIX NPs were previously developed and designed for theranostic approaches in cancer radiotherapy, with ultra-small size (under 5 nm). For the development of potential bimodal imaging systems, positron emitters are of special interest for patient selection, the development, and optimization of NPs radiolabeling is thus essential. Additionally, for enabling therapy planning and monitoring by PET imaging, the same drug delivery system should be radiolabeled with the corresponding therapeutic radionuclide. Radiolabeling with quite a variety of different PET isotopes have been developed and optimized in this work showing very favorable results. For the three PET/SPECT radionuclides considered, i.e. ^{67}Ga,^{44}Sc and ^{64}Cu, radiolabeling yields ranging from 60% to 100% could be reached, with no further purification. High specific activities were attainable for DOTA-based AGuIX NPs, regardless of the percentage of free DOTA at the surface of the NPs. These radiolabeled NPs have been evaluated for their integrity with regards to their size by HF5 analysis.

However, when dealing with the evaluation of nanoparticular systems for PET imaging, one should be aware of certain issues. The first issue concerns the synthesis of the structures and the decision of what labeling approach should be investigated or is suitable for the biological question asked (half-life; biological target). Successively, the radiolabeling becomes the prevalent question (direct labeling, prosthetic group labeling or *in situ* generation of the radionuclide) in sufficient radiochemical yields and in the right

formulation, i.e. volume activity and/or purification. Since all the physicochemical optimizations could be done, then *in vitro* and *in vivo* testing must be performed.

Preliminary investigations of AGuIX effectiveness have been performed to determine their pharmacokinetics, elimination pathway, metabolism, and potential degradation [59], showing *in vivo* safety. The next step is the use of the radiolabeling and PET/SPECT imaging platforms for systematic optimization of NPs towards specific applications.

Acknowledgements

The ARRONAX cyclotron is a project promoted by the Regional Council of Pays de la Loire financed by local authorities, the French government and the European Union. This work has been, in part, supported by a grant from the French National Agency for Research called "Investissements d'Avenir", Equipex Arronax-Plus no ANR-11-EQPX-0004 and Labex no ANR-11-LABX-0018-01.

Authors acknowledge Mrs. Veronique Sole-Jamault from INRA Nantes for the HF5 access and the FFF platform REFERENNS.

References

1. Acharya S, Sahoo SK (2011) PLGA nanoparticles containing various anticancer agents and tumour delivery by EPR effect. Adv Drug Deliv Rev 63: 170-183.
2. Lux F, Mignot A, Mowat P, Louis C, Dufort S, et al. (2011) Ultrasmall rigid particles as multimodal probes for medical applications. Angew Chem Int Ed 50: 12299-12303.
3. Le Duc G, Roux S, Paruta-Tuarez A, Dufort S, Brauer E, et al. (2014) Advantages of gadolinium based ultrasmall nanoparticles vs molecular gadolinium chelates for radiotherapy guided by MRI for glioma treatment. Cancer Nanotechnol 5: 4-9.
4. Sancey L, Kotb S, Truillet C, Appaix F, Marais A, et al. (2015) Long-Term in vivo clearance of Gadolinium-Based AGuIX (Activation and Guiding of Irradiation by X-Ray) Nanoparticles and their Biocompatibility after Systemic Injection. ACS Nano 9: 2477-2488.
5. Verry C, Dufort S, Barbier E, Montigon O, Peoc'h M, et al. (2016) MRI-guided clinical 6-MV radiosensitization of glioma using a unique gadolinium-based nanoparticles injection. Nanomed 11: 2405-2417.
6. Choi HS, Liu W, Liu F, Nasr K, Misra P, et al. (2010) Design considerations for tumour-targeted nanoparticles. Nat Nanotechnol 5: 42-47.
7. Choi HS, Frangioni JV (2010) Nanoparticles for biomedical imaging: Fundamentals of clinical translation. Mol Imaging 9: 291-310.
8. Wang L, Zhao W, Tan W (2008) Bioconjugated silica nanoparticles: Development and applications. Nano Res 1: 99-115.
9. Iyer AK, Khaled G, Fang J, Maeda H (2006) Exploiting the enhanced permeability and retention effect for tumor targeting. Drug Discov Today 11: 812-818.
10. Morlieras J, Dufort S, Sancey L, Truillet C, Mignot A, et al. (2013) Functionnalization of small rigid platforms with cyclic RGD peptides for targeting tumors overexpressing αvβ3 integrins. Bioconjugate Chem 24: 1584-1597.
11. Bechet D, Auger F, Couleaud P, Marty E, Ravasi L, et al. (2015) Multifunctionnal ultrasmall nanoplatforms for vascular-targeted interstitial photodynamic therapy of brain tumors guided by real-time MRI. Nanomedicine 11: 657-670.
12. Plissoneau M, Pansieri J, Heinrich-Balard L, Morfin JF, Stransky-Heilkron N, et al. (2016) Gd-nanoparticles functionalization with specific peptides for ß-amyloid plaques targeting. J Nanobiotechnol 14: 60-70.
13. Le Duc G, Miladi I, Alric C, Mowat P, Bräuer-Krisch E, et al. (2011) Toward an image-guided microbeam radiation therapy using gadolinium-based nanoparticles. ACS Nano 5: 9566-9574.
14. Morlieras J, Chezal JM, Miot-Noirault E, Vidal A, Besse S, et al. (2013) In vivo evidence of the targeting of cartilaginous tissue by pyridinium functionalized nanoparticles. Chem Commun 49: 3046-3048.
15. Price, EW, Orvig C (2014) Matching chelators to radiometals for radiopharmaceuticals. Chem Soc Rev 43: 260-290.
16. Mowat P, Mignot A, Rima W, Lux F, Tillement O, et al. (2011) In vitro radiosensitizing effects of ultrasmall gadolinium-based particles on tumour cells. J Nanosci Nanotechnol 11: 1-7.
17. Sancey L, Lux F, Kotb S, Roux S, Dufort S, et al. (2014) The use of theranostic gadolinium-based nanoprobes to improve radiotherapy efficacy. Br J Radiology 87: 20140134.
18. Mignot A, Truillet C, Lux F, Sancey L, Louis C, et al. (2013) A top-down synthesis route to ultrasmall multifunctional Gd-based silica nanoparticles for theranostic applications. Chem Eur J 19: 6122-6136.
19. Sumer B, Gao J (2008) Theranostic nanomedicine for cancer. Nanomedicine 3: 137-140.
20. Rechiglian P, Zattoni A, Cinque L, Roda B, Dal Piaz F, et al. (2004) Hollow-Fiber Flow Field-Flow Fractionation for Whole Bacteria Analysis by Matrix-Assisted Laser Desorption/Ionization Time-of-Flight Mass Spectrometry. Anal Chem 76: 2103-2111.
21. Cutler CS, Smith CJ, Ehrhardt GJ, Tyler TT, Jurisson SS, et al. (2000) Current and potential therapeutic uses of lanthanides radioisotopes. Cancer Biother Radiopharm 15: 531-545.
22. Paterson BM, Buncic G, McInnes LE, Roselt P, Cullinane C, et al. (2014) Bifunctional 64Cu-labelled macrobicyclic cage amine isothiocyanates for immuno-positron emission tomography. Dalton Trans 43: 1386-1396.
23. Uusijärvi H, Bernhardt P, Rösch F, Maecke HR, Forssell-Aronsson E (2006) Positron-Emitting Radiolanthanides for Therapy: Aspects of Dosimetry and Production. J Nucl Med 47: 807-814.
24. Niccoli Asabella A, Cascini GL, Altini C, Paparella D, Notaristefano A, et al. (2014) The Copper Radioisotopes: A Systematic Review with Special Interest to 64Cu. Biomed Res Int 2014: 786463.
25. Alliot C, Kerdjoudj R, Michel N, Haddad F, Huclier-Markai S (2015) Processing of a 44m/44Sc generator for potential medical applications: production and chemistry aspects. Nucl Med Biol 42: 524-529.
26. Prabhakar G, Joshi SH, Ranganatha DK, Umamaheswari S, Ananthakrishnan M, et al. (2000) Preparation and evaluation of samarium (III) phosphate [153Sm] colloid (SMPC) for possible therapeutic use. Nucl Med Biol 27: 353-356.

27. Cutler CS, Hennekens H, Nebiat S, Huclier-Markai S, Jurisson SS (2013) Radiometals for Combined Imaging and Therapy. Chem Reviews 113: 858-883.

28. Alliot C, Michel N, Bonraisin AC, Bossé V, Laizé J, et al. (2011) One step purification process for no-carrier-added 64Cu produced using enriched nickel target. Radiochim Acta 99: 627-630.

29. McCarthy DW, Shefer RE, Klinkowstein RE, Bass LA, Margeneau WH, et al. (1997) Efficient production of high specific activity 64Cu using a biomedical cyclotron. J Nucl Med Biol 24: 35-43.

30. Tanase M, Zolla V, Clement CC, Borghi F, Urbanska AM, et al. (2015) Hydrodynamic size-based separation and characterization of protein aggregates from total cell lysates. Nat Protoc 10: 134-148.

31. Truillet C, Bouziotis P, Tsoukalas C, Brugière J, Martini M, et al. (2015) Ultrasmall particles for Gd-MRI and 68Ga-PET dual imaging. Contrast Media Mol Imaging 10: 309-319.

32. Truillet C, Thomas E, Lux F, Huynh LT, Tillement O, et al. (2016) Synthesis and characterization of 89Zr-labeled ultrasmall nanoparticles. Mol Pharm 13: 2596-2601.

33. Martell AE, Smith RM (1989) Critical Stability Constants. Plenum Press, New York.

34. Miot-Noirault E, Vidal A, Morlieras J, Bonazza P, Auzeloux P, et al. (2014) Small rigid platforms functionalization with quaternary ammonium: targeting extracellular matrix of chondrosarcoma. Nanomedicine 10: 1887-1895.

35. Wadas TJ, Wong EH, Weisman GR, Anderson CJ (2010) Coordinating radiometals of copper, gallium, indium, yttrium and zirconium for PET and SPECT imaging of disease. Chem Rev 110: 2858-2902.

36. Hu F, Cutler CS, Hoffman T, Sieckman G, Volkert WA, et al. (2002) Pm-149 DOTA bombesin analogs for potential radiotherapy: in vivo comparison with Sm-153 and Lu-177 labeled DO3A-amide-betaAla-BBN(7-14)NH(2). Nucl Med Biol 29: 423-430.

37. Stimmel JB, Kull FC Jr (1998) Samarium-153 and Lutetium-177 Chelation Properties of Selected Macrocyclic and Acyclic Ligands. Nucl Med Biol 25: 117-125.

38. Locatelli E, Gil L, Israel LL, Passoni L, Naddaka M, et al. (2012) Biocompatible nanocomposite for PET/MRI hybrid imaging. Int J Nanomed 7: 6021-6033.

39. Huclier-Markai S, Kerdjoudj R, Alliot C, Bonraisin A, Michel N, et al. (2014) Optimization of reaction conditions for the radiolabeling of DOTA and DOTA-peptide with 44m/44Sc and experimental evidence of the feasibility of an in-vivo PET generator. Nucl Med Biol 41: e36-e43.

40. Pruszyski M, Majkowska-Pilip A, Loktionova N, Eppard E, Roesch F (2012) Radiolabeling of DOTATOC with the long-lived positron emitter 44Sc. Appl Rad Isot 70: 974-979.

41. Loktionova N, Filosofov D, Pruszynski M, Roesch F (2010) Design and performance of a novel 5 mCi 44Ti/44Sc radionuclide generator. J Nucl Med 51: 1467-1472.

42. Boros E, Ferreira CL, Cawthray JF, Price EW, Patrick BO, et al. (2010) Acyclic Chelate with Ideal Properties for 68Ga PET Imaging Agent Elaboration. J Am Chem Soc 132: 15726-15733.

43. Jalilian AR, Mirsadeghi L, Yari-kamrani Y, Rowshanfarzad P, Kamali-dehghan M, et al. (2007) Development of [64Cu]-DOTA-anti-CD20 for targeted therapy. Radioanal Nucl Chem 274: 563-568.

44. Yapp DT, Ferreira CL, Gill RK, Boros E, Wong MQ, et al. (2013) Imaging tumor vasculature noninvasively with positron emission tomography and RGD peptides labeled with copper 64 using the bifunctonal chelates DOTA, oxo-DO3a. and PCTA. Mol Imaging 12: 263-272.

45. Lewis JS, Laforest R, Lewis MR, Anderson CJ (2000) Comparative dosimetry of copper-64 and yttrium-90-labeled somatostatin analogs in a tumor-bearing rat model. Cancer Biother Radiopharm 15: 593-604.

46. Abadjian MC, Latoche J, Thomas E, Foley L, Day K, et al. (2016) PET and MR imaging with 64Cu/68Ga-labeled AGuIX ultra-small nanoparticles in tumor-bearing mice. J Nucl Med 57: 1181-1187.

47. Zhou M, Zhang R, Huang M, Lu W, Song S, et al. (2010) A chelator-free multifunctional [64Cu] CuS nanoparticle platform for simultaneous micro-PET/CT imaging and photothermal ablation therapy. J Am Chem Soc 132: 15351-15358.

48. Zhao Y, Sultan D, Detering L, Cho S, Sun G, et al. (2014) Copper-64-alloyed gold nanoparticles for cancer imaging: Improved radiolabel stability and diagnostic accuracy. Angew Chem Int Ed Engl 53: 156-159.

49. Wong RM, Gilbert DA, Liu K, Louie AY (2012) Rapid size-controlled synthesis of dextran-coated, 64Cu-doped iron oxide nanoparticles. ACS Nano 6: 3461-3467.

50. Yang X, Hong H, Grailer JJ, Rowland IJ, Javadi A, et al. (2011) cRGD-functionalized, DOX-conjugated, and 64Cu-labeled superparamagnetic iron oxide nanoparticles for targeted anticancer drug delivery and PET/MR imaging. Biomaterials 32: 4151-4160.

51. Glaus C, Rossin R, Welch MJ, Bao G (2010) In vivo evaluation of 64Cu-labeled magnetic nanoparticles as a dual-modality PET/MR imaging agent. Bioconjug Chem 21: 715-722.

52. Liu Q, Sun Y, Li C, Zhou J, Li C, et al. (2011) 18F-Labeled magnetic-upconversion nanophosphors via rare-Earth cation-assisted ligand assembly. ACS Nano 5: 3146-3157.

53. Ferrari M (2005) Cancer nanotechnology: opportunities and challenges. Nat Rev Cancer 5: 161-171.

54. Ga-67 Fact Sheet.

55. Kerdjoudj R, Pniok M, Alliot C, Kubicek V, Havlickova J, et al. (2016) Scandium(III) complexes of monophosphorus acid DOTA analogues: a thermodynamic and radiolabelling study with 44Sc from cyclotron and from a 44Ti/44Sc generator. Dalton Trans 45: 1398-1409.

56. Huang X, Zhang F, Lee S, Swierczewska M, Kiesewetter DO, et al. (2012) Long-term multimodal imaging of tumor draining sentinel lymph nodes using mesoporous silica-based nanoprobes. Biomaterials 33: 4370-4378.

57. Tu C, Ma X, House A, Kauzlarich SM, Louie AY (2011) PET Imaging and Biodistribution of Silicon Quantum Dots in Mice. ACS Med. Chem Lett 2: 285-288.

58. Lee DE, Na JH, Lee S, Kang CM, Kim HN, et al. (2013) Facile method to radiolabel glycol chitosan nanoparticles with 64Cu via copper-free click chemistry for Micro-PET imaging. Mol Pharm 10: 2190-2198.

59. Kotb S, Detappe A, Lux F, Appaix F, Barbier EL, et al. (2016) Gadolinium-Based Nanoparticles and Radiation Therapy for Multiple Brain Melanoma Metastases: Proof of Concept before Phase I Trial. Theranostics 6: 418-427.